Novel solid-state heavy rare-earth (III) picolinates: A pyrolytic study using: TG-DSC-FTIR, HSM-MS and GC-MS

A.L.C.S. Nascimento[a,b,1], G.P. Ashton[a], G.M.B. Parkes[a], B. Ekawa[b], R. P Fernandes[b], A. C. S. Carvalho[b], M. Ionashiro[b], F.J. Caires[b,c]

[a] *Thermal Methods Research Unit, School of Applied Sciences, University of Huddersfield, Queensgate, Huddersfield HD1 3DH, United Kingdom*

[b] *Instituto de Química, Universidade Estadual Paulista, CP 355, 14801-970 Araraquara, SP, Brazil*

[c] *Faculdade de Ciências , UNESP—Univ., Estadual Paulista, Campus Bauru, Departamento de Química, Bauru, SP 17033-260, Brazil*

Abstract

Heavy trivalent lanthanides and yttrium picolinates were synthesized by complexation of basic rare-earth metal carbonates with an aqueous solution of picolinic acid. The novel compounds were obtained with the general formula $Ln(L)_3 \cdot nH_2O$, where L is picolinate and n= 1.5 H_2O (Dy, Ho, Yb, Lu and Y), 2 H_2O (Tb and Tm) and 2.5 H_2O (Er). The stoichiometry of the complexes was calculated through mass losses found using thermogravimetry (TG), complexometry and elemental analysis (EA). The thermal behavior in oxidative and pyrolytic atmospheres of the compounds was analyzed by simultaneous thermogravimetry - differential scanning calorimetry (TG-DSC). The gaseous products of the pyrolysis were determined throughout by monitoring the evolved species using TG-DSC, Fourier transform infrared spectroscopy (TG-DSC-FTIR), hot-stage microscopy mass spectrometry (HSM-MS), and gas chromatography-mass spectrometry (GC-MS). The obtained results validated mass loss assignments made using the TG curves. However, gaseous product analysis indicates the degradation processes are more complex than the thermoanalytical techniques suggest alone. This study used a GC-MS technique to identify the condensed gaseous products obtained during the second step of the thermal degradation of the picolinate complexes. The analysis of the symmetric and asymmetric stretching frequencies of the carboxylate group in the FTIR spectra showed a monodentate bonding mode. The compounds were obtained in the amorphous state, as indicated by the powder X-ray diffractometry (PXRD) data.

Keys works: Heavy trivalent lanthanide picolinates, evolved gas analysis (EGA), TG-DSC-FTIR, HSM-MS, GC-MS.

[1] **Corresponding author.**
e-mail address: nascimento.a.l.c@gmail.com

Introduction

Picolinic acid ($C_6H_5NO_2$) is a substance found widely in nature, particularly in plants and humans, participating in key regulatory processes and provides assimilation of elements [1]. Complexes using picolinates have therapeutic uses in both humans and animals, for example chromium picolinate may be used as a dietary supplement, with the complex also being reported to reduce morphine dependence in rats [2-3]. Zinc picolinate was also studied as a dietary supplement, aiming to reduce the oxidative stress found in species of rainbow trout [4]. A variety of picolinate complexes have been described in the literature using a wide range of metal centers including Cu, Mn, Rh, Ir, and many others [5–9].

Moreover, picolinate has uses as a sensitizer, assisting the provision of luminescence to selected lanthanides (i.e. europium and terbium), which affords mechanoluminescent complexes [10]. Studies implementing the complexation of trivalent rare-earth with derivatives of picolinate have also been explored, aiming to further improve the luminescence and the energy transfer between the ligand and lanthanide [11-12]. The literature reports the functionalization of picolinates to form compounds such as; dipicolinate, N-oxide picolinate [13–18], 3-hydroxypicolinate, and 3,5-dipicolinate, as well as the introduction of picolinate on a triazacyclononane ring system [13–17], studies about picolinate salts with rare-earth were also found [19].

Spectroscopic studies of some light-lanthanides have suggested that picolinate complex binds through the nitrogen in the pyridine ring and with the carboxylate group [20]. The same mode of coordination is observed for the dysprosium [21] and terbium [19] complexes that bind monodentatively with the carboxylate group.

In another study, holmium was found binding in a bidentate bridging mode with additional bonding to the pyridine nitrogen atom [22]. To the best of our knowledge, comprehensive studies determining the thermal behavior of heavy trivalent ions with picolinate remain unexplored. The understanding of the thermal and pyrolytic decomposition of heavy picolinates is essential in the event that these compounds are made into functional materials which may operate in unknown thermal environments.

This work extends on our previous studies on light trivalent lanthanide picolinates [20] and reports the synthesis of heavy trivalent lanthanide (Tb to Lu) and yttrium (III) picolinates. The investigation and characterisation of these novel compounds were carried out using a range of thermoanalytical, chromatographic, spectrometric and spectroscopic techniques.

Experimental

Materials

Picolinic acid ($C_6H_6NO_2$, 99.5%) was obtained from Sigma and was used without further purification. Aqueous solutions of heavy lanthanide (Tb to Lu and Y) chlorides were prepared

from the corresponding metal oxides (Aldrich ≥ 99%), by treatment with concentrated hydrochloric acid (Merck, 37%), following the previously described procedure [20].

Due to solubility issues of heavy trivalent lanthanide picolinates, the respective basic carbonates were obtained prior to the formation of the picolinate complexes. The basic carbonates of heavy trivalent lanthanides and yttrium(III) were prepared as previously described [23]. Solid-state compounds were prepared by mixing the corresponding metal basic carbonates with an aqueous solution of picolinic acid in non-stoichiometric conditions. The basic carbonates were kept in slight excess to prevent picolinic acid contamination, which was observed previously when used in a 1: 1 ratio.

The aqueous suspension was heated up to ebullition until total neutralization of the acid, cooled to room temperature, and filtered to remove the basic carbonate in excess. Thus, the aqueous solutions of the respective (Tb to Lu and Y) picolinates were evaporated to near dryness in a water bath, dried at 50 °C in an air-circulated oven for 12h, and finally kept in a desiccator over anhydrous calcium chloride.

Following the procedure established to the light lanthanide picolinates [20], any precipitate was observed to heavy series (all of them have high aqueous solubility). Other synthetic routes were tried without success which may explain why some of these compounds are unreported.

EDTA (Sigma, ≥ 99 %) solutions were prepared for complexometry studies.

Equipment and conditions

In the solid-state, hydration water, metal ions and picolinate contents were determined from TG curves. Complexometry studies were carried out by firstly driving the individual compounds to their respective oxides through high temperature exposure (1000 °C, 1h). The oxides were then dissolved in a solution of hydrochloric acid and the concentration of metal ions was determined using a standard EDTA solution following a previously reported method [24,25].

Carbon, nitrogen and hydrogen contents were determined by microanalytical procedures, with a CNH elemental analyzer model 2400 from Perkin-Elmer and from TG curves, since the total mass loss occurs with the formation of residue with known stoichiometry.

The DSC curves were obtained with DSC Q10 from TA instruments. The purge gas was nitrogen flow of 50 mL min^{-1}. A heating rate of 10 C min^{-1} was adopted with samples weighing about 3 mg in aluminum crucibles with a perforated lid.

Simultaneous TG-DSC curves were obtained by using a TG-DSC 1 Star^e system (Mettler Toledo). The purge gas was dry air or nitrogen with a flow of 50 mLmin^{-1}. A heating rate of 10°C min^{-1} was adopted, with samples weighing about 10mg. Alumina crucibles were used for recording the TG-DSC curves.

Powder x-ray diffractometry patters were obtained by using the Siemens D-5000 X-ray diffractometer, employing CuKα radiation (λ= 1,541Å) and setting of 40 kV and 20 mA. Temperature dependent studies were performed on terbium picolinate. Individual samples of

terbium picolinate were heated at 280 °C, 330 °C and 350 °C using a hot-stage system (described later), PXRD analysis was performed after homogenizing in an agate pestle and mortar.

Infrared spectra were obtained by using an is10 FTIR spectrophotometer (Nicolet), utilizing an ATR accessory with Ge window. The FTIR spectra were recorded with 32 scans per spectrum at resolution of 4 cm^{-1}.

The EGA (TG-FTIR) experiments were performed using a TG-DSC (Mettler Toledo) coupled to a FTIR spectrophotometer (Nicolet). A gas cell held at 250 °C was coupled through a heated (225 °C) 120 cm stainless steel line transfer with diameter of 3 mm, both purged with dry air (50 $mLcm^{-1}$). The FTIR spectra were recorded with 16 scans per spectrum at a resolution of 4 cm^{-1}, approximating to one full scan per degree Celsius represented by Gram-Schmidt curves.

Hot-stage microscopy (HSM) measurements were performed using a system developed at Huddersfield [26] following the procedures previously described [27]. Samples (10 mg) were placed in alumina crucibles and heated at a rate of 10 °C min^{-1} under an inert atmosphere of helium. Micrographs were recorded every 10 °C. The HSM system was coupled to a quadrupole mass spectrometer (HPR20, Hiden, Warrington, UK) operated in EI mode. Evolved sample gases were transferred via a heated quartz capillary line (250 °C) to the inlet of the spectrometer; full mass scans were recorded between 4 and 300 mass units with an accumulation time of 200 ms per scan.

GC-MS method developed to evaluate EGA condensates

Approximately 15 mg of sample was weighed to single-sealed 100 mm x 1 mm glass tube. The samples were encouraged to the bottom and then sealed using a butane burner. The sealed tubes were stationed in muffle furnace set to 330 °C (deemed ideal following the previous thermoanalytical temperature screen) and heated at this temperature for 20 minutes.

Once fully cooled to room temperature, a yellow condensed was observed in the upper part of the tubes. An aliquot of 2.0 mL of methanol (LCMS grade, Fisher) was used to remove the condensed part. The samples were then kept on ultrasound for 1 minute to encourage the maximum dissolution of degradation products. The resulting solutions were transferred to GC-MS via filtration over cotton wool and analyzed with methanol as the blank.

GC-MS analysis was performed on Agilent 7890A-5975C gas chromatograph coupled to a quadrupole mass spectrometer. The temperatures of the injector and the interface line were 250 °C and 280 °C, respectively. Chromatographic separation was achieved on a 30 m x 0.25 mm x 0.25 µm HP-5ms Ultra Inert capillary column (Alltech, Carnforth,0 UK) under the following conditions: 40 °C for 2 min, then 5 °C min^{-1} to 100 °C, then 20 °C min^{-1} to 325 °C and hold for 5 min. Injections (1 mL) were made in the split mode with a 50:1 split ratio. Helium at a head pressure of 7.1 psi was used as the carrier gas and the capillary column was connected directly to the ion source of the mass spectrometer. The mass spectrometer was operated in the EI mode under SIM conditions with the following source parameters: electron energy 70 eV, emission current 300 mA and source temperature 230°C.

Results and discussion

Table 1. Analytical and thermoanalytical (TG*) data for $Ln(L)_3.nH_2O$ compounds.

Compounds	Metal oxide/ %			L (Lost)/ %		H_2O/ %		C (%)			N (%)			H (%)			Final Residue
	Calc.	TG	EDTA	Calc.	TG	Calc.	TG	Calc.	EA	TG	Calc.	EA	TG	Calc.	EA	TG	
$Tb(L)_3{\cdot}2\ H2O$	33.30	32.90	32.72	64.41	65.20	6.42	6.00	37.32	36.99	37.26	7.26	6.94	7.25	2.52	2.60	2.54	Tb_4O_7
$Dy(L)_3{\cdot}1.5H2O$	33.55	33.81	33.47	64.73	64.58	4.86	5.48	36.52	36.90	36.60	7.10	7.53	7.06	2.45	2.49	2.46	Dy_2O_3
$Ho(L)_3{\cdot}1.5H2O$	33.84	33.73	33.55	64.44	64.74	4.84	4.83	37.51	38.01	37.08	7.29	6.55	7.21	2.44	2.51	2.45	Ho_2O_3
$Er(L)_3{\cdot}2.5\ H2O$	33.05	33.76	33.54	64.16	63.76	7.78	7.77	34.66	35.15	34.57	6.74	7.40	6.72	2.53	2.42	2.51	Er_2O_3
$Tm(L)_3.\ 2\ H2O$	33.77	33.99	34.08	63.96	63.86	6.31	6.53	37.84	37.41	37.66	7.36	7.30	7.33	2.48	2.35	2.46	Tm_2O_3
$Yb(L)_3{\cdot}1.5\ H2O$	34.79	34.92	35.02	63.47	63.24	4.77	4.73	36.99	37.50	37.17	7.19	6.79	7.22	2.41	2.42	2.40	Yb_2O_3
$Lu(L)_3{\cdot}1.5\ H2O$	34.95	35.20	35.40	63.30	62.56	4.76	5.44	37.48	37.97	37.62	7.29	6.66	7.32	2.40	2.45	2.33	Lu_2O_3
$Y(L)3{\cdot}1.5\ H2O$	23.41	23.40	23.98	75.20	74.53	5.60	5.85	43.21	43.82	43.00	8.40	8.94	8.36	2.83	2.97	2.81	Y_2O_3

*TG in air atmosphere, Ln = Heavy Lanthanides and Yttrium, L = Picolinate.

The elemental analysis (EA) and thermogravimetric (TG) data for the synthesized compound are shown in Table 1. The EA and TG results are in close agreement with each other and support the stoichiometry: $Ln(L)_3{\cdot}nH_2O$, Ln = (Tb to Lu and Y), L = picolinate and *n*= 1.5 H_2O (Dy, Ho, Yb, Lu and Y), 2 H_2O (Tb and Tm) and 2.5 H_2O (Er).

The powder X-ray patterns showed that all compounds were obtained in the amorphous state (Fig SI1).

The attenuated total reflectance infrared spectroscopic data on picolinate (sodium salt) and the complexes with heavy trivalent lanthanides and yttrium ions are shown in the supplementary material (Fig SI2). This study focused mainly around the 1700-1400 cm^{-1} region which had the most informative data relating to the coordination sites. Key frequencies of interest are shown in Table 2.

Table 2. Spectroscopic data for sodium picolinate and compounds with heavy trivalent lanthanide metal ions considered in this work.

Compounds	ν_{as} (COO^-) cm^{-1}	ν_s (COO^-) cm^{-1}	$\Delta\nu cm^{-1}$
NaL	1564s	1390m	174
$Tb(L)_3{\cdot}2H_2O$	1618s	1372m	246
$Dy(L)_3{\cdot}1.5H_2O$	1618s	1372m	246
$Ho(L)_3{\cdot}1.5H_2O$	1619s	1372m	247
$Er(L)_3{\cdot}2{,}5H_2O$	1621s	1371m	250
$Tm(L)_3{\cdot}2H_2O$	1622s	1372m	250
$Yb(L)_3{\cdot}1.5H_2O$	1623s	1372m	251
$Lu(L)_3{\cdot}1.5H_2O$	1624s	1373m	251
$Y(L)_3{\cdot}1.5H_2O$	1624s	1373m	251

L = picotinate; s = strong; m = medium.
ν_{as} (COO^-) = antisymmetric carboxyl stretching frequency.
ν_s (COO^-) = symmetric carboxyl stretching frequency.
$\Delta\nu$ = difference between ν_{as} (COO^-) and ν_s (COO^-) frequencies.

In sodium picolinate, medium-intensity band at 1564 cm^{-1} and strong band at 1390 cm^{-1} are attributed to the antisymmetric (ν_{as} COO^-) and symmetric (ν_s COO^-) stretching frequencies of carboxylate groups, respectively as previously reported[28,29]. The synthesized heavy picolinate compounds show that the same frequencies are extended between 1700 and 1300 cm^{-1}. Analysis of the frequencies of the ν_{as} COO^- and ν_s COO^- indicates that the coordination is being carried out through the carboxylate [28], the FTIR data suggest that the bonding of the carboxylate group to metal is monodentate [30] in agreement with other workers [9,21] and our previous study of the light trivalent lanthanide picolinates [20].

Thermal behavior in oxidative atmosphere

The simultaneous TG-DSC curves of the compounds in dynamic dry air atmosphere are shown in Figure 1 (a - h). All the compounds show mass losses in five steps. Endothermic peaks are attributed to dehydration and thermal decomposition, whilst exothermic peaks attributed to oxidation of the organic matter and/or of the gaseous products evolved during thermal decomposition.

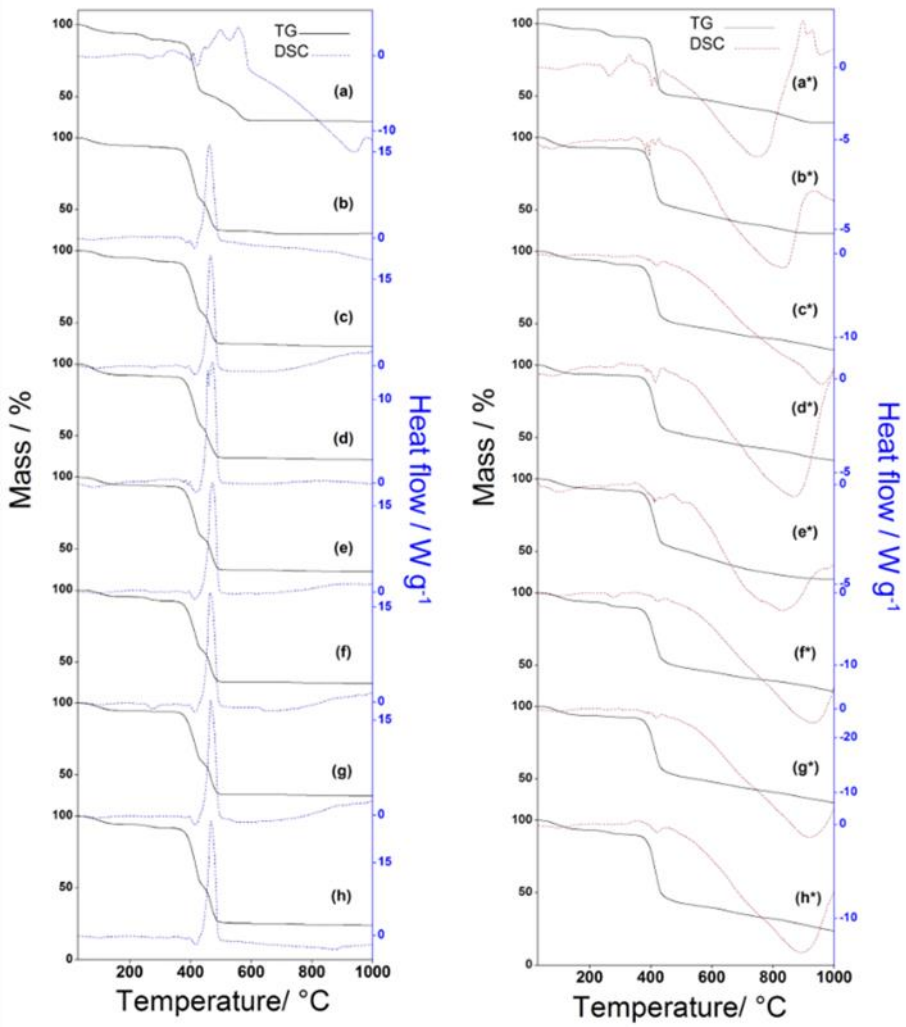

Figure 1. TG-DSC curves in dry air (a-h) and N_2 (a*-h*) atmospheres of the picolinates, being: a and a* = Tb; b and b* = Dy; c and c* = Ho; d and d* = Er; e and e* = Tm, f and f* = Yb; g and g* = Lu; h and h* = Y.

TG-DSC curves of all compounds show a single slow mass loss step, corresponding to the endothermic event between 30 and 170 °C, attributed to the loss of weakly bound water molecules.

Once dehydrated, the thermal decomposition of the anhydrous compounds occurs in four consecutive steps.

For all the studied compounds, the second mass loss occurs slowly. Accompanying the secondary mass loss, small endothermic events are noted. We believe these endotherms arise from thermal degradation/rearrangements of the lanthanide picolinates (as supported by the EGA data below). This is in disagreement with earlier literature suggesting that this step relates to further dehydration of coordinated water molecules [21].

The third steps occur through a fast mass loss process and have corresponding endothermic events on the DSC curves. The process has been attributed to a melt and onset of thermal decomposition of the remaining material, highlighted further in the supplementary video (SI-3) obtained from the HSM with all compounds showing an apparent melt except for the terbium picolinate.

The fourth step (occurring as a shoulder of the third) shows a sharp mass loss from all compounds (with the exception of terbium) with a highly exothermic peak concluding by 520 °C. The processes have been attributed to the oxidation of the remaining organic matter and release of gaseous products. At this stage the remaining material is expected to have to formed carbonaceous and dioxycarbonate residues of the form $Ln_2O_2CO_3$ (Ln = heavy lanthanides considered in this work), as previously reported for light-picolinates [20].

The fifth and final mass loss step occurs slowly above 490 °C, with a variety of corresponding thermal events forming the final oxide residues. Oxidation of carbonaceous residue gave exothermic events, whilst thermal decomposition of the dioxycarbonates gave endothermic responses.

Terbium picolinate follows a similar degradation profile to the other picolinates until the mass loss events between 310 °C and 600 °C. Prior to the third mass loss step, an exothermic process (340 °C) is noted which has been attributed to a crystallisation process (confirmed using PXRD as discussed below). Although endothermic events (395 and 420 °C) are observed during the third mass loss no apparent melting was observed using HSM (SI3) which is clearly different to the other picolinates. The overlapping fourth and fifth mass losses show exothermic events (495 and 550 °C) as the remaining carbonaceous residues are oxidatively removed leaving behind Tb_4O_7, a degradation reaction that has previously been observed for terbium compounds [31,32].

To summarise; the total mass loss up to 600 °C is in agreement with the formation of Tb_4O_7 as residue (Calc. = 66.70%, TG = 67.28%). The total mass loss up to 720 °C (Dy), 880 °C (Ho), 860 °C (Er), 920 °C (Tm, Yb and Lu) and 940 °C (Y) are in agreement with the formation of Ln_2O_3 as final residue (Ln = Dy-Lu and Y).

Table 3 summarises the TG-DSC data for the experiments in an oxidative atmosphere. The mass losses, temperatures ranges and peak temperatures observed in each step were found to be characteristic of each compound.

Table 3. Temperatures ranges (ΔT), mass losses (Δm) and peak temperatures (T_P) observed for each step of TG-DSC curves of the $Ln(L)_3 \cdot nH_2O$ compounds in dynamic dry air atmosphere, where Ln = heavy-lanthanides and yttrium, L = picolinate. The arrows indicate whether a particular process is exothermic or endothermic.

Compounds		Steps				
		First	Second	Third	Fourth	Fifth
$Tb(L)_3 \cdot 2H_2O$	ΔT/ °C	30 - 170	230 - 270	310 - 430	430 - 500	500 - 600
	Δm/ %	6.00	4.60	35.75	7.40	12.93
	T_P/ °C	90↓	265↓	340↑ 395↓ 420↓	495↑	550↑
$Dy(L)_3 \cdot 1.5H_2O$	ΔT / °C	30 - 170	180 - 300	310 - 425	425 - 510	510 - 720
	Δm/ %	5.48	1.28	35.26	21.77	2.23
	T_P/ °C	80 ↓	270 ↓	385 ↓ 410 ↓	455 ↑	_____
$Ho(L)_3 \cdot 1.5H_2O$	ΔT /°C	30 - 170	215 - 295	330 – 435	435 - 500	500 - 880
	Δm/ %	4.80	2.34	38.05	22.35	1.77
	T_P/ °C	100 ↓	280 ↓	385 ↓ 415 ↓	455 ↑	_____
$Er(L)_3 \cdot 2.5H_2O$	ΔT / °C	30 -170	190 - 290	320 - 430	430 - 520	520 - 860
	Δm/(%)	7.69	0.87	34.49	22.11	1.02
	T_P/(°C)	90↓	_____	375↓ 390↓ 415 ↓	450 ↑ 465 ↑	_____
$Tm(L)_3 \cdot 2H_2O$	ΔT / °C	30 - 170	230 - 310	330 - 430	430 - 490	490 - 920
	Δm/ %	5.53	0.72	34.41	22.84	1.68
	T_P/ °C	100 ↓	270 ↓	380 ↓ 410 ↓	465 ↑	_____
$Yb(L)_3 \cdot 1.5H_2O$	ΔT / °C	30 - 170	210 - 310	330 - 430	430 - 500	500 - 920
	Δm/ %	4.70	2.86	32.97	23.14	1.10
	T_P/ °C	100 ↓	275 ↓	380 ↓/ 415 ↓	455 ↑	_____
$Lu(L)_3 \cdot 1.5H_2O$	ΔT / °C	30 - 170	240 - 290	335 - 435	435 - 525	525 - 920
	Δm/ %	5.32	0.55	33.99	23.19	1.64
	T_P/ °C	100 ↓	_____	380 ↓/ 415 ↓	460 ↑	_____
$Y(L)_3 \cdot 1.5H_2O$	ΔT / °C	30 - 170	215 -285	330 - 430	430 - 545	545 – 940
	Δm/ %	5.75	2.20	38.97	27.07	1.96
	T_P/ °C	100 ↓	270 ↓	385 ↓/ 415 ↓	460 ↑	_____

Pyrolysis

The simultaneous TG-DSC curves in dynamic dry nitrogen atmosphere are shown in Fig 1 (a*-h*). All the curves show mass losses in five steps and endothermic events attributed to dehydration, thermal decomposition or pyrolysis of the compounds.

Terbium, dysprosium and thulium compounds show final mass loss occurring through a slow process up to 930 °C (Tb), 910 °C (Dy) and 960 °C (Tm) and the total mass losses up to these temperatures are in agreement with the formation of the respective oxides, Tb_2O_3, Dy_2O_3 and Tm_2O_3, respectively.

For the other compounds, the last step also occurs through a slow process; however, the mass loss had not completed by 1000 °C thus a formula mass assignment could not be given.

In all the compounds, the first mass loss is attributed to dehydration. The dehydrated compounds then exhibit mass losses in four consecutive steps, with the last two overlapping. The first step after dehydration is similar to that observed for the experiments performed in an oxidative atmosphere. It occurs through a slow process corresponding to thermal decomposition as confirmed by EGA experiments (see below).

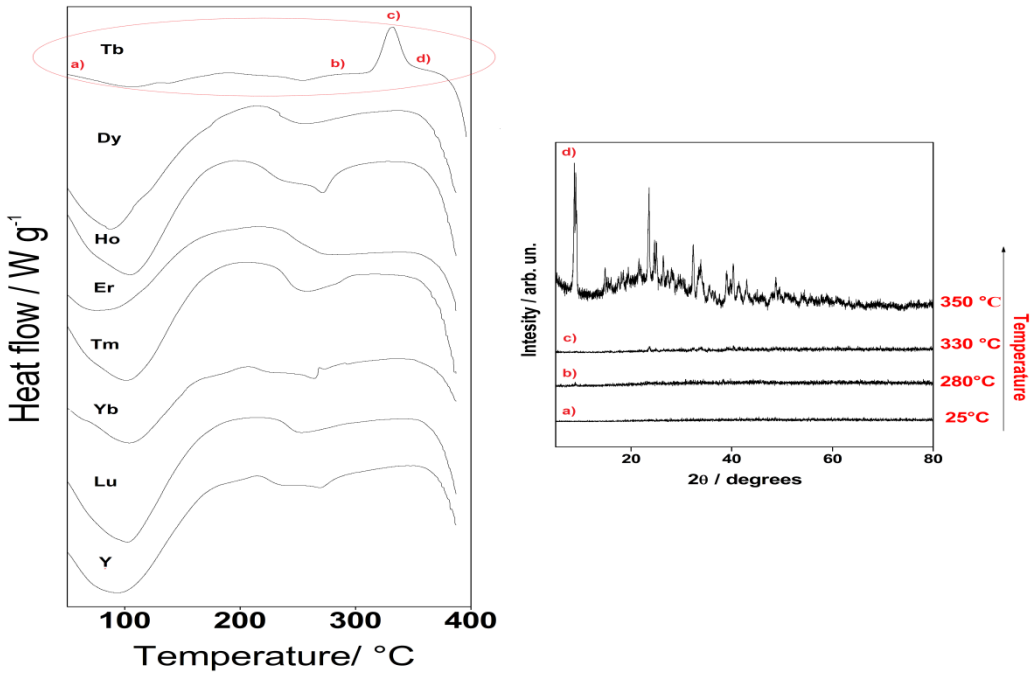

Figure 2- DSC curves of heavy picolinates and PXRD from terbium picolinate in each step of thermal decomposition (a) 25°C, (b) 280°C, (c) 330°C, (d) 350°C

Figure 2 shows the DSC curves up to 400 °C and the powder X-ray diffractograms obtained at different temperatures and shows the unique behavior of the terbium complex.

As previously discussed and as observed by HSM, terbium picolinate undergoes decomposition followed by crystallization of the anhydrous compound. Therefore, PXRD analysis was performed at room temperature, before, during and after crystallization process. As the temperature increases, the formation of Bragg peaks is shown, indicating the formation of

crystalline material from the previous amorphous state (Fig 2a-d) with a strong resemblance between it and other anhydrous crystalline picolinates [20]. The powder X-ray diffractogram confirms sample crystallization is at 350 °C. The associated energy of crystallization was found to be 73.96 J g^{-1} using DSC.

Summarising the findings of Figure 1. (a*-h*). The first and second mass losses appear independent of the atmosphere, as such occur in the same manner as the previously described. The third mass loss of the compounds occurs through a fast process, corresponding to an endothermic peak attributed to the thermal decomposition with the formation of carbonaceous residue. The last two overlapping steps (enhanced by DTG analysis) occur through slow processes and have been attributed to the pyrolysis of the remaining carbonaceous residue. Table 4 summarises the TG-DSC data for the experiments in a pyrolytic atmosphere. The mass losses, temperatures ranges and peak temperatures observed in each step were again found to be characteristic of each compound.

Table 4. Temperatures ranges (ΔT), mass losses (Δm) and peak temperatures (T_P) observed for each step of TG-DSC curves of the $Ln(L)_3 \cdot nH_2O$ compounds in dynamic dry nitrogen atmosphere, where Ln = heavy-lanthanides and Yttrium, L = picolinate. The arrows indicate whether a particular process is exothermic or endothermic.

Compounds		Steps				
		First	Second	Third	Fourth	Fifth
$Tb(L)_3 \cdot 2H_2O$	ΔT/ °C	30 - 170	180 - 300	310 - 435	435 - 700	700 - 930
	Δm/ %	3.64	5.23	38.81	10.38	10.72
	T_P/ °C	100 ↓	265 ↓	330↑ 400↓ 420↓	_____	750 ↓ 930 ↓
$Dy(L)_3 \cdot 1.5H_2O$	ΔT/ °C	30 - 170	122 - 310	330 - 430	435 - 720	720 - 910
	Δm/ %	6.97	0.58	36.58	15.52	6.32
	T_P/ °C	55 ↓ 85 ↓	_____	380↓ 390↓ 410↓	_____	830↓
$Ho(L)_3 \cdot 1.5H_2O$	ΔT/°C	30 – 170	190 – 290	330 - 430	430 - 730	730 - > 1000
	Δm/ %	6.07	3.27	35.64	13.83	9.77
	T_P/ °C	100 ↓	280 ↓	385↓ 415↓	_____	960↓
$Er(L)_3 \cdot 2.5H_2O$	ΔT/ °C	30 – 170	200 - 290	330 - 435	435 - 695	695 - >1000
	Δm/(%)	6.03	0.87	35.83	12.63	10.47
	T_P/(°C)	90 ↓	260 ↓	380↓ 390↓ 415↓	_____	870↓
$Tm(L)_3 \cdot 2H_2O$	ΔT/ °C	30 - 170	180 - 330	330 - 435	435 - 700	700 - 960
	Δm/ %	6.15	1.64	35.56	17.91	7.66
	T_P/ °C	110↓	250↓	410↓ 435↓	500↓	830↓
$Yb(L)_3 \cdot 1.5H_2O$	ΔT/ °C	30 - 170	200 - 310	330 - 440	440 - 735	735 - > 1000
	Δm/ %	5.97	3.80	36.31	12.90	8.73
	T_P/ °C	110↓	275↓	420↓	_____	930↓
$Lu(L)_3 \cdot 1.5H_2O$	ΔT/ °C	30 - 170	180 - 290	340 - 435	435 - 700	700 - > 1000
	Δm/ %	6.08	1.18	34.85	13.41	10.20
	T_P/ °C	100↓	255↓	405↓ 410↓ 415↓	_____	920↓
$Y(L)_3 \cdot 1.5H_2O$	ΔT/ °C	30 - 170	200 - 290	320 - 440	440 - 710	710 - > 1000
	Δm/ %	6.47	2.80	41.98	13.42	11.15
	T_P/ °C	100↓	275↓	415↓	_____	890↓

Evolved gas analysis (EGA)

The gaseous products evolved during the thermal decomposition of the compounds were monitored by the EGA techniques: TG-DSC-FTIR, HSM-MS and GC-MS. The main gaseous products found were water, pyridine, carbon monoxide and carbon dioxide, in both atmospheres and in agreement with our previous findings [20]. The major differences arise between the heavy-picolinates and the light-lanthanide picolinates are the latter are anhydrous. The mass spectrometric techniques show that the process may be more complex than at first indicated by FTIR alone.

TG-DSC-FTIR

The FTIR spectra of gaseous products evolved during the thermal decomposition under N_2 atmosphere of erbium picolinate (representative of all the complexes studied) are shown in Figure 3. Water release can be seen for all the compounds up to the dehydration temperature (Figure 3 a-1 and b-1) as indicated by the presence of 4000-3500 cm^{-1} and also 2000-800 cm^{-1} bands.

A release of pyridine (near to 3000 cm^{-1} and 1500 cm^{-1}), carbon monoxide (between 2250-2000 cm^{-1}) and carbon dioxide (near to 2300 cm^{-1}) is observed during mass losses. The region 2 is represented by the increase of intensity in the Gram Schmidt curve at 23 min (260 °C) with release of CO_2 and pyridine (Figure 3 a-2). This experiment confirms that second step of all the compounds can be attributed to thermal decomposition, in disagreement with the secondary dehydration suggested by other workers [21].

Figure 3c shows a 3D graphic of FTIR spectra obtained during the experiment. The higher absorbance seen at 40 min (430 °C) corresponds to the major mass loss step observed at this temperature with TG-DSC.

Finally, during region 4 at 63 min (660 °C), release of CO and CO_2 is observed until the end of the experiment indicating the ongoing pyrolysis of carbonaceous residue and in confirmation with the previous TG-DSC data.

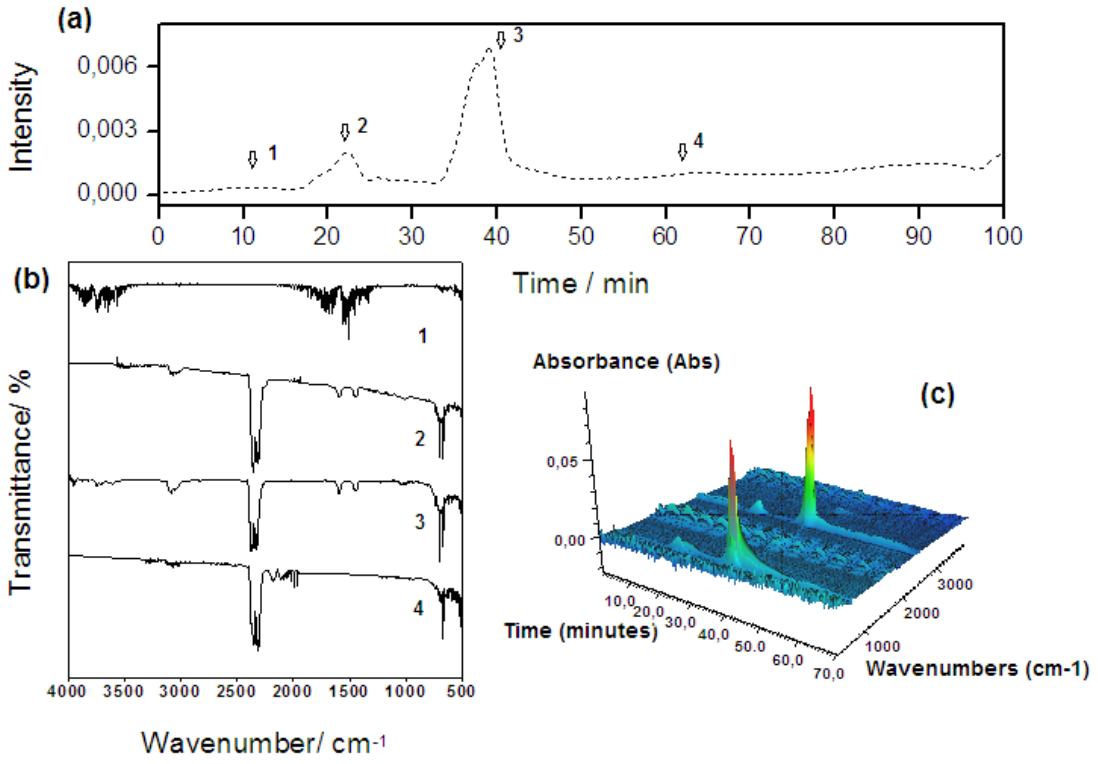

Figure 3- (a) Gram Schmidt curve, (b) infrared spectra and (c) FTIR 3D graphic of erbium picolinate.

HSM- MS

The pyrolysis of erbium picolinate in a helium atmosphere (used to enhance MS sensitivity) was monitored by HSM-MS and used as representative for all the compounds presented in Figure 4.

Three key gaseous compounds are plotted: water ($[M]^{+\cdot}$ 18 *m/z*), carbon dioxide ($[M]^{+\cdot}$ 44 *m/z*) and pyridine ($[M]^{+\cdot}$ 79 *m/z*). The presence of pyridine was confirmed by monitoring the pyridine fragment ions (26, 27, 39 and 52 *m/z*) as compared with the NIST MS database.

Water can be seen to be evolved over the broad dehydration range 30 to 180 °C in agreement with the first mass loss described earlier. The evolution of the water signal occurs over the majority of the temperature range, the observed pyrolytic mass loss processes are typically broad as shown in the earlier TG-DSC studies. Carbon dioxide is observed during *ca.* 185 °C while pyridine is not observed until *ca.* 240 °C. At *ca.* 380 °C both carbon dioxide and pyridine are evolved simultaneously.

Figure 4 also shows an average mass spectrum over the 400-420 °C temperature range where the largest mass loss occurs. The average mass spectrum is in agreement with the NIST database for both pyridine and carbon dioxide.

A video obtained from micrographs recorded every 10 °C is given in the supplementary material. No optical changes were observed during dehydration. However, color changes, vapour release and sample compaction were observed for all compounds during the second step. The third step showed an apparent melting for all complexes with the exception for terbium, in agreement with earlier TG-DSC data.

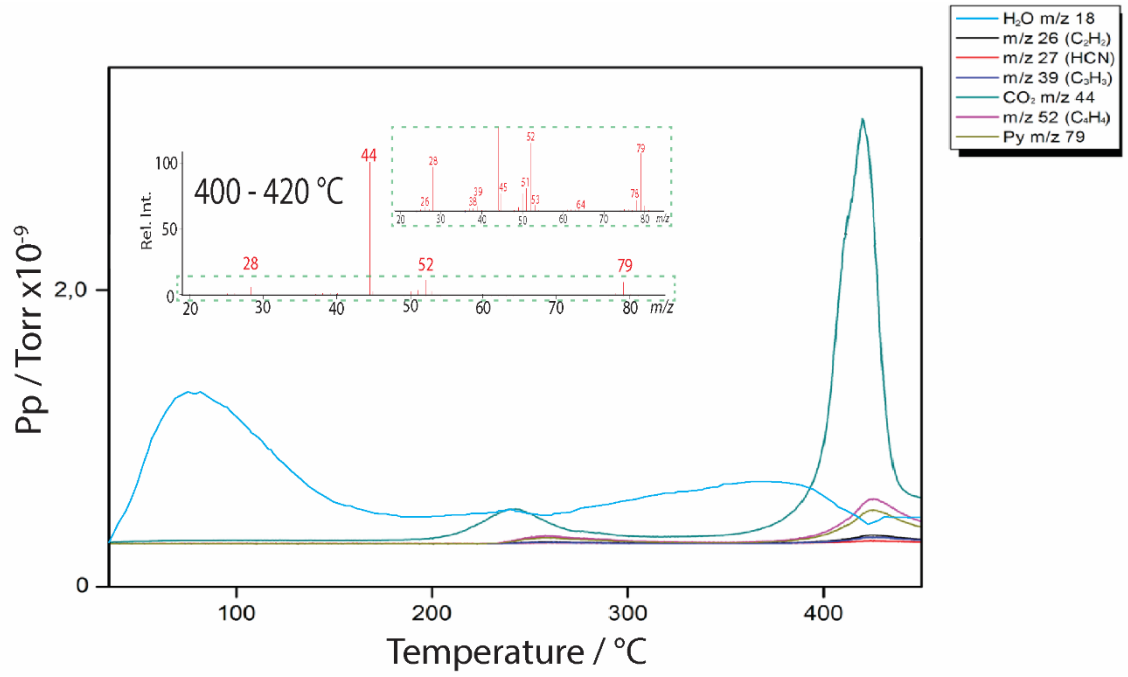

Figure 4. Selected ion (shown in the key) mass spectral data obtained from HSM-MS analysis of erbium picolinate. Figure insert shows average and expanded (checkered box) mass spectra over the 400 to 420 °C region.

GC-MS

Figure 5 shows the chromatogram and average mass spectra obtained for the condensed gaseous products collected between the two stages discussed previously using TG-DSC-FTIR and HSM-MS. Four compounds were identified in the chromatogram of the condensate products.

The peak at 4.3 minutes was identified as pyridine using the NIST database in agreement with the earlier EGA experiments.

No other compounds were observed in the chromatogram until the 18.5-19.5 minutes region, where 2,2'-Bipyridine (18.8 mins), 2,2'-Methylenebipyridine (19.2 mins) and 2,4-Bipyridine (19.5 mins) were identified again through comparisons with the NIST database. All compounds had strong agreement with few discrepancies between experimental and database values (94 %, 93 %, 94 % and 85 % matches respectively). These compounds were not apparent using the other EGA techniques and it is possible that these are actually products of a reaction owing to the higher concentration of gaseous pyridine and naturally higher pressures in a sealed ampoule. However, since the ratio of these products to the dominating pyridine signal were very low (84:7:7:2 ratio) the other techniques are likely to have been significantly less sensitive to these trace compound levels.

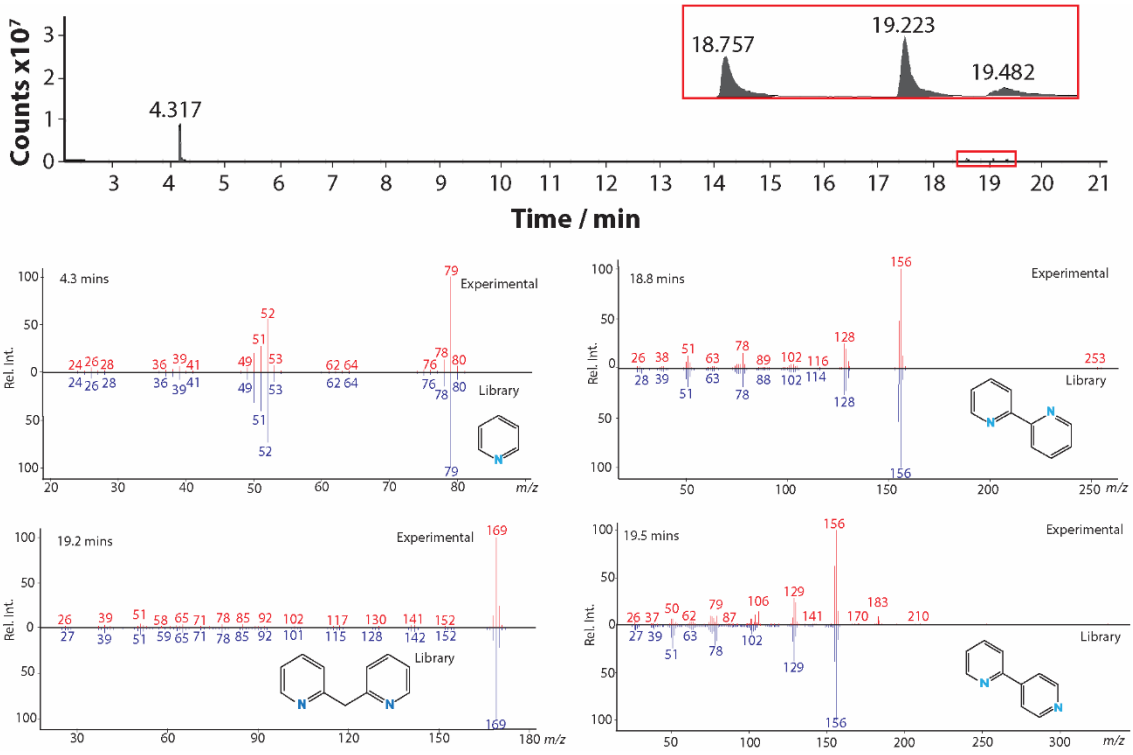

Figure 5. GC-MS data obtained from erbium picolinate condensates, collected at 330 °C. *Upper*) TIC chromatogram for analysed condensates. *Lower*) Experimental and library (inverted) average mass spectra for; pyridine (4.3 mins), 2,2'-Bipyridine (18.8 mins), 2,2'-Methylenebipyridine (19.2 mins) and 2,4-Bipyridine (19.5 mins)

Conclusions

Basic heavy-lanthanide carbonates obtained by precipitation in a homogeneous medium using urea as neutralizing agent were mixed in non-stoichiometric conditions with picolinic acid giving a novel synthesis route for the preparation of heavy lanthanide picolinate complexes.

Thermoanalytical techniques, complexometry and elemental analysis, demonstrate that synthesised heavy lanthanide picolinate complexes have the general formula: $Ln(L)_3 \cdot nH_2O$,

whereby Ln = (Tb to Lu and Y), L = picolinate and *n* = (1.5, 2 or 2.5). PXRD indicated that all compounds were amorphous.

FTIR analysis of the symmetrical and asymmetrical stretching of carboxylate group suggests that the coordination of picolinate ion is through a monodentate binding regime as has been previously reported for the light-lanthanide picolinates.

TG-DSC experiments show the compounds undergo complex degradation under both pyrolytic and oxidative atmospheres. All samples, with the exception of terbium, gave very similar profiles although there were small differences in key transitional temperatures. Under a pyrolytic atmosphere only terbium, dysprosium and thulium were completely decomposed to their respective oxides. Under oxidative conditions all heavy-lanthanide picolinates formed their respective oxides with the general formula Ln_2O_3. However, the terbium complex was found to form a crystalline material with the formula Tb_4O_7 irrespective of the atmosphere.

Pyrolytic TG-DSC-FTIR analysis of heavy-lanthanide picolinates shows the release of carbon dioxide, carbon monoxide and pyridine. The observed temperature of degradation after dehydration was lower than has been previously reported.

HSM-MS provided both physical and chemical information during the pyrolytic degradation of picolinate complexes. All complexes were shown to melt prior to decomposition with the exception of the terbium complex. The MS provided enhanced and complementary information to support the TG-DSC-FTIR findings.

A sample preparation method which effectively generates and retains thermal degradation products of the picolinate metal complexes was successfully developed. Following this, a GC-MS method which shows clear and effective separation of all signals from condensated degradation material was utilized.

Acknowledgments

The authors thanks University of Huddersfield, FAPESP, CNPq and CAPES Foundations (Brazil) for financial support. This research was supported by resources supplied by PDSE from CAPES Foundation (Proc.88,881.135291/2016-01).

References

[1] G. Świderski, M. Kalinowska, J. Malejko, W. Lewandowski, Spectroscopic (IR, Raman, UV and fluorescence) study on lanthanide complexes of picolinic acid, Vib. Spectrosc. 87 (2016) 81–87. doi:10.1016/j.vibspec.2016.09.012.

[2] B. Liu, Y. Liu, J. Chai, X. Hu, D. Wu, B. Yang, Chemical properties and biotoxicity of several chromium picolinate derivatives, J. Inorg. Biochem. 164 (2016) 110–118. doi:10.1016/j.jinorgbio.2016.09.006.

[3] D. Ciubotariu, M. Nechifor, G. Dimitriu, Chromium picolinate reduces morphine-

dependence in rats, while increasing brain serotonin levels, J. Trace Elem. Med. Biol. 50 (2018) 676–683. doi:10.1016/j.jtemb.2018.06.025.

[4] Z. Kucukbay, H. Yazlak, N. Sahin, M. Tuzcu, M. Nuri Cakmak, F. Gurdogan, V. Juturu, K. Sahin, Zinc picolinate supplementation decreases oxidative stress in rainbow trout (Oncorhynchus mykiss), Aquaculture. 257 (2006) 465–469. doi:10.1016/j.aquaculture.2006.03.005.

[5] C. Biswas, A.D. Jana, M.G.B. Drew, G. Mostafa, A. Ghosh, Segregated self-assembly and pillaring action of aliphatic dicarboxylic acids in the super structure of Cu-picolinate complexes, Polyhedron. 28 (2009) 653–660. doi:10.1016/j.poly.2008.11.061.

[6] Ö. Tamer, D. Avci, Y. Atalay, B. Çoşut, Y. Zorlu, M. Erkovan, Y. Yerli, Synthesis, crystal structure, spectroscopic characterization and nonlinear optical properties of manganese (II) complex of picolinate: A combined experimental and computational study, J. Mol. Struct. 1106 (2016) 98–107. doi:10.1016/j.molstruc.2015.10.077.

[7] S. Basu, S.M. Peng, G.H. Lee, S. Bhattacharya, Synthesis, structure and electrochemical properties of tris-picolinate complexes of rhodium and iridium, Polyhedron. 24 (2005) 157–163. doi:10.1016/j.poly.2004.10.015.

[8] E. Callens, A.J. Burton, A.J.P. White, A.G.M. Barrett, Mechanistic study on benzylic oxidations catalyzed by bismuth(III) salts: X-ray structures of two bismuth-picolinate complexes, Tetrahedron Lett. 49 (2008) 3709–3712. doi:10.1016/j.tetlet.2008.04.044.

[9] Ö. Tamer, D. Avci, Y. Atalay, Synthesis, X-ray structure, spectroscopic characterization and nonlinear optical properties of Nickel (II) complex with picolinate: A combined experimental and theoretical study, J. Mol. Struct. 1098 (2015) 12–20. doi:10.1016/j.molstruc.2015.05.035.

[10] J.C.G. Bünzli, K.L. Wong, Lanthanide mechanoluminescence, J. Rare Earths. 36 (2018) 1–41. doi:10.1016/j.jre.2017.09.005.

[11] J.C.G. Bünzli, A.S. Chauvin, H.K. Kim, E. Deiters, S. V. Eliseeva, Lanthanide luminescence efficiency in eight- and nine-coordinate complexes: Role of the radiative lifetime, Coord. Chem. Rev. 254 (2010) 2623–2633. doi:10.1016/j.ccr.2010.04.002.

[12] V.F. Zolin, V.I. Tsaryuk, V.A. Kudryashova, K.P. Zhuravlev, P. Gawryszewska, J. Legendziewicz, R. Szostak, Spectroscopy of Eu3+and Tb3+pyridine- and pyrazine-2-carboxylates, J. Alloys Compd. 451 (2008) 149–152. doi:10.1016/j.jallcom.2007.04.125.

[13] A. De Bettencourt-Dias, P.S. Barber, S. Viswanathan, Aromatic N-donor ligands as chelators and sensitizers of lanthanide ion emission, Coord. Chem. Rev. 273–274 (2014) 165–200. doi:10.1016/j.ccr.2014.04.010.

[14] L.J. Xu, G.T. Xu, Z.N. Chen, Recent advances in lanthanide luminescence with metal-organic chromophores as sensitizers, Coord. Chem. Rev. 273–274 (2014) 47–62. doi:10.1016/j.ccr.2013.11.021.

[15] M.L. Cable, D.J. Levine, J.P. Kirby, H.B. Gray, A. Ponce, Luminescent lanthanide sensors, 2011. doi:10.1016/B978-0-12-385904-4.00010-X.

[16] L. Armelao, S. Quici, F. Barigelletti, G. Accorsi, G. Bottaro, M. Cavazzini, E. Tondello, Design of luminescent lanthanide complexes: From molecules to highly efficient photo-emitting materials, Coord. Chem. Rev. 254 (2010) 487–505.

doi:10.1016/j.ccr.2009.07.025.

[17] P. Guerriero, U. Casellato, S. Sitran, P.A. Vigato, R. Graziani, Preparation and properties of lanthanide complexes with pyridine-2,6-dicarboxylic and thiophene-2,5-dicarboxylic acids. Crystal structure of diaqua-bis(dipicolinate)lanthanum(III) tetrahydrate, Inorganica Chim. Acta. 133 (1987) 337–345. doi:10.1016/S0020-1693(00)87789-0.

[18] J. Mao, H. Zhang, J. Ni, T.C.W. Mak, Synthesis and crystal structure of a polymeric erbium (III)— sodium (I) coordination complex of picolinic acid N-oxide, 28 (1998) 413–418.

[19] D. Sendor, M. Hilder, T. Juestel, P.C. Junk, U.H. Kynast, One dimensional energy transfer in lanthanoid picolinates. Correlation of structure and spectroscopy, New J. Chem. 27 (2003) 1070–1077. doi:10.1039/b302499g.

[20] A.L.C.S. Do Nascimento, J.A. Teixeira, W.D.G. Nunes, F.X. Campos, O. Treu-Filho, F.J. Caires, M. Ionashiro, Thermal behavior, spectroscopic study and evolved gas analysis (EGA) during pyrolysis of picolinic acid, sodium picolinate and its light trivalent lanthanide complexes in solid state, J. Anal. Appl. Pyrolysis. 119 (2016) 242–250. doi:10.1016/j.jaap.2016.01.010.

[21] M. Jian-Fang, H. Ning-Hai, N. Jia-Zuan, Structure of hydrated dysprosium picolinate, [Dy(C5H4NCO2)3(H2O)2]2.8H2O, Polyhedron. 15 (1996) 1797–1799. doi:10.1016/0277-5387(95)00435-1.

[22] P. Starynowicz, Structure of ethylenediammonium catena-poly[tris(2-pyridinecarboxylato-κN,κO)holmate-μ-2-pyridinecarboxylato-κN,κO:κO']hexahydrate, Acta Crystallogr. Sect. C Cryst. Struct. Commun. 49 (1993) 1895–1897. doi:10.1107/S0108270193004603.

[23] L.M. D'Assunção, I. Giolito, M. Ionashiro, Thermal decomposition of the hydrated basic carbonates of lanthanides and yttrium, Thermochim. Acta. 137 (1989) 319–330. doi:10.1016/0040-6031(89)87224-7.

[24] H.A. Flaschka, EDTA Titrations, Elsevier, 1964. doi:10.1016/C2013-0-07757-2.

[25] M. Ionashiro, Titulação complexométrica de lantanídeos e ítrio, Eclética Química J. 8 (1983) 29. doi:10.26850/1678-4618eqj.v8.1.1983.p29-32.

[26] B. Berger, A.J. Brammer, E.L. Charsley, Thermomicroscopy studies on the zirconium-potassium perchlorate-nitrocellulose pyrotechnic system, Thermochim. Acta. 269–270 (1995) 639–648. doi:10.1016/0040-6031(95)02671-1.

[27] A.L.C.S. Nascimento, G.M.B. Parkes, G.P. Ashton, R.P. Fernandes, J.A. Teixeira, W.D.G. Nunes, M. Ionashiro, F.J. Caires, Thermal analysis in oxidative and pyrolysis conditions of alkaline earth metals picolinates using the techniques: TG-DSC, DSC, MWTA, HSM and EGA (TG-DSC-FTIR and HSM-MS), J. Anal. Appl. Pyrolysis. 135 (2018) 67–75. doi:10.1016/j.jaap.2018.09.018.

[28] K. Nakamoto, Infrared and Raman Spectra of Inorganic and Coordination Compounds, John Wiley & Sons, Inc., Hoboken, NJ, USA, 2008. doi:10.1002/9780470405840.

[29] R.M. Silverstein, F.X. Webster, D.J. Kiemle, D.D. Bryce, Spectrometric Identification of Organic Compounds, 8th ed., Wiley, 2014.

[30] G. Deacon, R.J. Phillips, Relationships between the carbon-oxygen stretching frequencies

of carboxylato complexes and the type of carboxylate coordination, Coord. Chem. Rev. 33 (1980) 227–250. doi:10.1016/S0010-8545(00)80455-5.

[31] J.A. Teixeira, W.D.G. Nunes, A.L.C.S. do Nascimento, T.A.D. Colman, F.J. Caires, D.A. Gálico, M. Ionashiro, Synthesis, thermoanalytical, spectroscopic study and pyrolysis of solid rare earth complexes (Eu, Gd, Tb and Dy) with p -aminobenzoic acid, J. Anal. Appl. Pyrolysis. 121 (2016) 267–274. doi:10.1016/j.jaap.2016.08.006.

[32] F.J. Caires, D.J.C. Gomes, A.C. Gigante, M. Ionashiro, Thermal investigation and infrared evolved gas analysis of solid trivalent lanthanide and yttrium α-hydroxyisobutyrates in N2 and CO2 atmospheres, J. Anal. Appl. Pyrolysis. 107 (2014) 313–322. doi:10.1016/j.jaap.2014.04.001.